EJN European Journal of Neuroscience

FENS Federation of European Neuroscience Societies

European Journal of Neuroscience, pp. 1–15, 2015 doi:10.1111/ejn.12849

Spatio-temporal dynamics of adaptation in the human visual system: a high-density electrical mapping study

Gizely N. Andrade,[1,2] John S. Butler,[1,3] Manuel R. Mercier,[1] Sophie Molholm[1,2] and John J. Foxe[1,2,3]

[1]Departments of Pediatrics and Neuroscience, The Sheryl and Daniel R. Tishman Cognitive Neurophysiology Laboratory, Children's Evaluation and Rehabilitation Center (CERC), Albert Einstein College of Medicine, Van Etten Building – Wing 1C, 1225 Morris Park Avenue, Bronx, NY 10461, USA

[2]Departments of Psychology & Biology, The Graduate Center of the City University of New York, New York, NY, USA

[3]Trinity Centre for Bioengineering and Trinity College Institute of Neuroscience, Trinity College, Dublin 2, Ireland

Keywords: EEG, habituation, inhibition, plasticity, vision

Abstract

When sensory inputs are presented serially, response amplitudes to stimulus repetitions generally decrease as a function of presentation rate, diminishing rapidly as inter-stimulus intervals (ISIs) fall below 1 s. This 'adaptation' is believed to represent mechanisms by which sensory systems reduce responsivity to consistent environmental inputs, freeing resources to respond to potentially more relevant inputs. While auditory adaptation functions have been relatively well characterized, considerably less is known about visual adaptation in humans. Here, high-density visual-evoked potentials (VEPs) were recorded while two paradigms were used to interrogate visual adaptation. The first presented stimulus pairs with varying ISIs, comparing VEP amplitude to the second stimulus with that of the first (paired-presentation). The second involved blocks of stimulation ($N = 100$) at various ISIs and comparison of VEP amplitude between blocks of differing ISIs (block-presentation). Robust VEP modulations were evident as a function of presentation rate in the block-paradigm, with strongest modulations in the 130–150 ms and 160–180 ms visual processing phases. In paired-presentations, with ISIs of just 200–300 ms, an enhancement of VEP was evident when comparing S2 with S1, with no significant effect of presentation rate. Importantly, in block-presentations, adaptation effects were statistically robust at the individual participant level. These data suggest that a more taxing block-presentation paradigm is better suited to engage visual adaptation mechanisms than a paired-presentation design. The increased sensitivity of the visual processing metric obtained in the block-paradigm has implications for the examination of visual processing deficits in clinical populations.

Introduction

Adaptation of neural responses to invariant or repetitive environmental inputs is a fundamental property of sensory processing, believed to represent a mechanism by which sensory systems attenuate representational redundancy (Müller *et al.*, 1999; Wissig & Kohn, 2012; Cattan *et al.*, 2014). Adaptation typically manifests as a rapid attenuation of neural responsiveness, providing a good metric of short-term neural plasticity. The hypothesized reduction in representational redundancy likely serves to enhance the brain's ability to detect more relevant novel environmental changes. Visual adaptation can be examined by comparing changes in the amplitude of the visual-evoked potential (VEP) to repetition at varying presentation rates. Terminology in the field is not always consistent, with such VEP adaptation effects sometimes referred to as 'habituation' or 'sensory gating'. Adaptation to presentation rates can be calculated across pairs of consecutive trials by comparing VEP amplitudes between the first and second stimulus of a pair (Adler *et al.*, 1985). Alternatively, comparisons can be made between VEPs elicited by trains of stimuli presented at fixed rates, where rate is varied across blocks of trials (Megela & Teyler, 1979).

In humans, adaptation to repetitive auditory stimulation has been extensively studied and is now quite well characterized (Fruhstorfer *et al.*, 1970; Potter *et al.*, 2006; Rosburg *et al.*, 2010; Chang *et al.*, 2011; Grzeschik *et al.*, 2013; Lanting *et al.*, 2013). A main finding in both auditory habituation and gating studies has been that the shorter the period between stimulus presentations, the greater the attenuation observed (Roth *et al.*, 1976; Budd *et al.*, 1998; Muller-Gass *et al.*, 2008; Rosburg *et al.*, 2010; Pereira *et al.*, 2014). Although the mechanisms behind auditory adaptation are not fully understood, several studies implicate local mechanisms such as neuronal refractoriness and presynaptic calcium influx, particularly in paired-presentation designs. Also implicated are top-down mechanisms related to expectancy, sensory memory and novelty detection, particularly when more than two stimuli are used, such as in a block design. These plasticity mechanisms are thought to involve *N*-methyl-D-aspartate (NMDA)-mediated glutamate transmission, γ-aminobutyric acid (GABA)-ergic inhibition and changes in the

Correspondence: Dr J. J. Foxe, [1]Department of Pediatrics and Neuroscience, as above.
E-mail: john.foxe@einstein.yu.edu

Received 18 September 2014, accepted 31 December 2014

ongoing oscillatory activity of the brain (e.g. in the gamma band frequency; Zucker, 1989; Chung *et al.*, 2002; Friston, 2005; Grill-Spector *et al.*, 2006; Brockhaus-Dumke *et al.*, 2008; Orekhova *et al.*, 2008; Carlén *et al.*, 2012). In contrast, studies of adaptation to visual stimulation are relatively sparse and have yielded inconsistent and even contradictory findings.

Here, we set out to comprehensively map adaptation functions of the visual system in healthy adults using high-density electrical mapping techniques. Most of the previous literature has been limited to low-density montages, and there has been a strong tendency to focus on amplitude changes at discrete VEP components, providing a somewhat static view of what is undoubtedly a dynamic ongoing process. This, along with a bias towards paired-presentation paradigms and a lack of studies examining VEP adaptation to simple presentation rate manipulations, has provided an incomplete picture of visual adaptation processes.

In the auditory and somatosensory systems, the amplitude of the neural response dramatically attenuates following repeated rapid paired-stimulation (McLaughlin & Kelly, 1993; Hetrick *et al.*, 1996; Arnfred *et al.*, 2001; Braff *et al.*, 2007), although it should be noted that the auditory-evoked potential (AEP) can also increase in response to the second stimulus in a pair when very short inter-stimulus intervals (ISIs) are employed (Loveless *et al.*, 1989, 1996). In vision, findings are considerably less clear-cut. For example, there are reports of strong adaptation to paired-stimuli using monocular stimulation (Wastell & Kleinman, 1980b), while others report weakened adaptation to binocularly presented paired-stimuli as compared with other sensory modalities (Davis *et al.*, 1972), and yet others report adaptation effects to paired-stimuli that are specific to right lateral occipital scalp-sites (Gjini *et al.*, 2008). On the other hand, there are also reports of adaptation effects over bilateral occipital scalp to non-identical, spatially segregated stimuli (Gawne *et al.*, 2011). Given the differences in the experimental paradigms used to assess visual adaptation to paired-stimuli, it is difficult to form a coherent picture of which effects are consistent, and what variables are driving these effects.

In block-stimulation designs, the picture is equally confusing. For example, Wastell & Kleinman (1980a,b) conducted a pair of studies that highlight the effects of both paradigm and presentation rate on VEP adaptation. In varying the amount of time between stimulus presentations within a train of 10 trials, they showed significantly more adaptation (i.e. VEP attenuation) in 'fast' conditions (500 and 1000 ms ISIs) compared with 'slow' conditions (2000 and 3000 ms ISIs; Wastell & Kleinman, 1980a). In the second of their studies, a paired-presentation design with monocular stimulation was employed, and attenuation was observed in ipsilaterally and contralaterally elicited VEPs with an ISI of 1000 ms (Wastell & Kleinman, 1980b). Still other studies failed to show any rapid adaptation effects in the visual domain in healthy controls or in patients with chronic schizophrenia when employing a paired-presentation paradigm (Adler *et al.*, 1985).

Clearly, much remains to be done to adequately characterize the adaptation properties of the human visual system. There is an added imperative to map visual adaptation properties, as visual processing and sensory adaptation deficits may serve as strong candidate endophenotypes for various psychiatric disorders. In schizophrenia, for instance, the P1 component of the VEP is attenuated in first-episode drug-naive patients, chronic patients, and their first-degree unaffected relative (Foxe *et al.*, 2001; Yeap *et al.*, 2006, 2008a,b). Furthermore, patients with schizophrenia consistently display altered auditory adaptation (Adler *et al.*, 1985; Potter *et al.*, 2006; Braff *et al.*, 2007; Patterson *et al.*, 2008), but visual adaptation functions have yet to be closely interrogated in this population. Evidence is also emerging for visual-sensory processing abnormalities in individuals with an autism spectrum disorder (Frey *et al.*, 2013). We believe that under adequately taxing conditions, a second-order measure of 'dynamic' early visual processing may offer a unique window into specific, observable short-term plasticity and sensory processing, with implications for characterizing psychiatric and neurodevelopmental disorders. However, before addressing deficits in a clinical population, the spatial and temporal profile of visual adaptation in the healthy visual system must be fully elucidated. Questions remain as to how quickly the VEP attenuates, which regions of the visual cortex show the greatest adaptation effects, when during the temporal evolution of the sensory processing period adaptation effects emerge, how different paradigms affect adaptation, how adaptation is affected by presentation rate, and how detectible all these changes are to non-invasive measuring techniques.

We examined these questions here in a pair of related experiments. Experiment 1 involved presenting pairs of stimuli with varying ISIs and comparing the amplitude of the VEP to the second stimulus with that of the first (paired-presentation) as a function of ISI. Experiment 2 involved presenting stimuli at a constant ISI in blocks of 100 stimuli, and then comparing the VEP amplitude across blocks for different ISIs (block-presentation). The major goals of this study were the following: (1) to assess whether visual adaptation can be assayed employing parameters similar to those used in somatosensory and auditory studies, as measured by the paired-presentation paradigm (Experiment 1); (2) whether further taxation of the system in the block-presentation paradigm (Experiment 2) results in a differing adaption profile; (3) whether studying second-order 'dynamic' characteristics of the brain, such as VEP adaptation changes elicited by different stimulus presentation rates and across various scalp-sites, would offer additional understanding of sensory processing in the visual system (Experiments 1 and 2); (4) whether adaptation functions are robust enough to be statistically identified at the individual participant level; and (5) to employ inverse source-localization techniques to estimate the major cortical generators of adaptation effects.

Materials and methods

Participants

Eleven healthy adults (four males, mean age = 26 years, SD = 3.6) completed Experiment 1. Fifteen healthy adults completed Experiment 2 (eight males, mean age = 26 years, SD = 4.4). Of the 15 participants in Experiment 2, three also completed Experiment 1. All had normal or corrected-to-normal vision. The experimental procedures were approved by the Institutional Review Board at Albert Einstein College of Medicine and conformed to the tenets of the Declaration of Helsinki. All participants provided written informed consent and received a modest fee.

Stimuli

Stimuli were 100% contrast black and white checkerboard annuli (6.5 cm diameter, 1 cm width, 4 ° × 4 °, white luminance of 120 cd/m^2, black luminance of 0.2 cd/m^2) centered against a gray (luminance = 25 cd/m^2) background. A fixation cross was always present on the screen, including during checkerboard presentation. The fixation cross changed color every 20–40 s. Checkerboards were presented for 33 ms and at different ISIs.

Procedure

Participants sat in a darkened sound-attenuated electrically shielded double-walled booth (Industrial Acoustics Company, Bronx, NY, USA), 90 cm from a 34 × 55 cm LCD computer screen (ViewSonic VP2655wb, 60 Hz refresh rate). They were instructed to minimize head movements and blinking while fixating on a red cross at the center of the screen. They performed a change detection task to ensure fixation in which they were asked to respond to fixation cross color changes (from red to green, lasting 40 ms) with a mouse button press using the index finger of their dominant hand. The presentation of checkerboard stimuli was temporally unrelated to this central fixation task.

Paradigms

Experiment 1: paired-presentation

Participants were presented with the checkerboard stimuli in pairs (first stimulus in pair = S1, second stimulus in pair = S2) with an ISI of either 200 ms or 300 ms. There was a 2500 ms interval between the paired-presentations. A non-paired stimulus (i.e. a 'catch' trial) was randomly presented one-third of the time during a semi-random time point (> 2500 ms) in the inter-pair interval. Subjects were exposed to approximately 300 presentations of each condition (pair with 200 ms ISI, pair with 300 ms ISI, and catch). The total run time for this experiment ranged from 45 to 60 min.

Experiment 2: block-presentation

Checkerboards were presented in blocks of 100 stimuli. Within each block, the stimuli were centered at an ISI, around which the actual presentations were jittered by ± 50 ms. Five different ISIs were used: 200 ms, 300 ms, 550 ms, 1050 ms and 2550 ms. For example, the following sequence of ISIs might be typical of a segment of trials in the 300 ms ISI condition: 272–267–304–320–336–300–288, etc. The between-block interval was self-paced, with participants allowed to move to the next block by pressing the spacebar on a keyboard 2500–5000 ms after the last stimulus of the preceding block. Block-presentation was pseudorandom. In total, participants experienced four blocks of each of the four shorter ISIs (200 ms, 300 ms, 550 ms, 1050 ms) and two blocks of the longest ISI (2550 ms). The total run time for the experiment ranged from 35 to 45 min (for a schematic time course representation of Experiments 1 and 2, see Fig. 1).

Data acquisition

Continuous electroencephalographic (EEG) data were recorded in both experiments using a Biosemi ActiveTwo 168-channel electrode

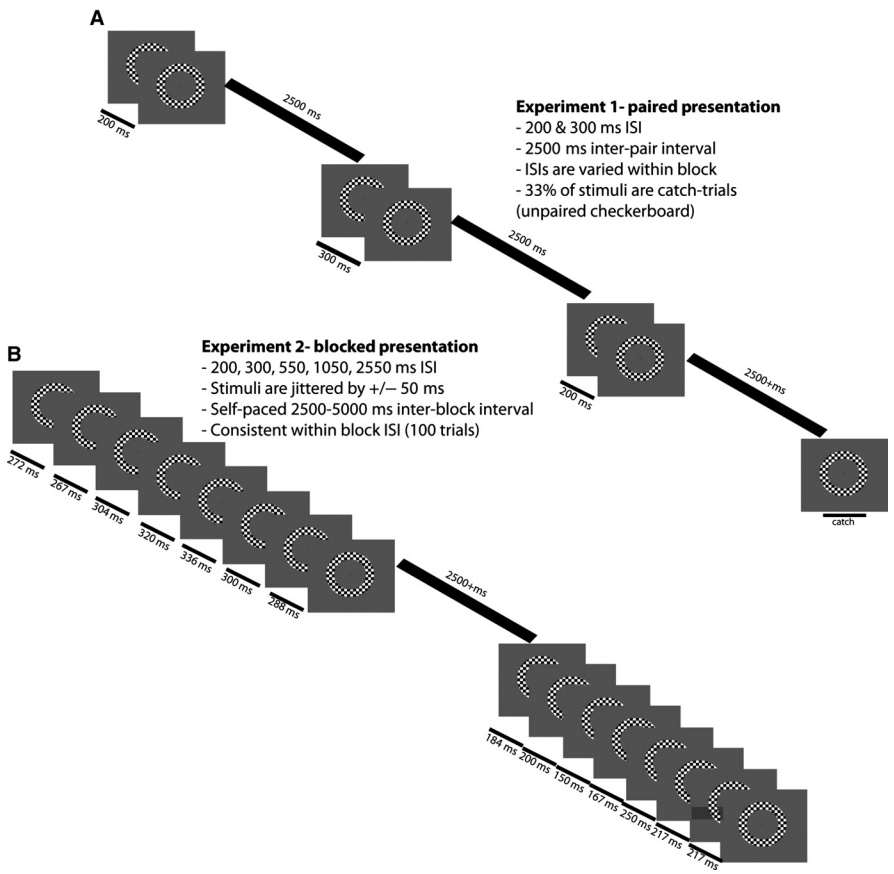

FIG. 1. Schematic diagram illustrating the two paradigms. (A) Depiction of the paired-presentation paradigm used in Experiment 1. Stimuli were presented in pairs with an inter-stimulus interval (ISI) of either 200 ms or 300 ms and a long inter-pair interval of 2500 ms. Catch trials, consisting of unpaired checkerboards, were presented one-third of the time and were used to extract the isolated response to the second stimulus in a pair. (B) Depiction of the block-presentation paradigm used in Experiment 2. Stimuli were presented in blocks of 100 trials, at an ISI centered around ISIs of 200, 300, 550, 1050 or 2550 ms. The stimulus presentation was jittered by ± 50 ms to allow for the implementation of an ADJAR procedure that models and removes response overlap (used in the 200 ms condition).

array, analog-to-digital converter, and fiber-optic pass-through to a dedicated data acquisition computer. The data were recorded at 512 Hz with a pass-band from DC to 150 Hz. The continuous EEG was subsequently low-pass filtered at 45 Hz (fourth order-zero phase Butterworth filter, 27 dB/octave) and high-pass filtered at 1 Hz (fourth order-zero phase Butterworth filter, 24 dB/octave). Epochs of 600 ms with 100 ms prestimulus baseline were extracted from the continuous data. An automatic artifact rejection criterion of ± 75 μV was applied across all electrodes in the array. Trials with more than six artifact channels were rejected. In trials with less than six such channels, any remaining bad channels were interpolated using the nearest neighbor spline (Perrin *et al.*, 1987; Butler *et al.*, 2011). The data were re-referenced to the average of all channels.

Pre-processing

Experiment 1: catch trial transformation

For the paired-presentation experiment (Experiment 1), waveforms for the S2 VEP were derived to isolate the responses to the S2 from the continued activity related to the S1, due to the short ISIs used. These waveforms were derived by subtracting the 'catch' from the composite S1–S2 VEP and then shifting the isolated S2 response back in time by the appropriate delay (see Fig. S1 for an illustration of the catch trial transformation). The subtraction allowed for the examination of the 'pure' VEP response to the second stimulus in a pair without any interference from ongoing activity related to the first stimulus. There was an average acceptance rate of 74% of trials per condition for this experiment.

Experiment 2: adjacent response (ADJAR) algorithm

As the timing between the stimuli of the shortest ISI was between 150 and 250 ms, we implemented the ADJAR algorithm on our subject-level data to model and remove any response overlap (Woldorff, 1993; Fiebelkorn *et al.*, 2013). ADJAR correction was only applied to the 200 ms ISI condition (see Fig. S2 for a depiction of data from the 200 ms ISI condition before and after the ADJAR procedure). There was an average acceptance rate of 82% of trials per condition for this experiment.

Analysis strategy

Identifying scalp-sites of interest and time-windows for primary analysis

For each experiment, the data from all participants from each electrode were collapsed into a single averaged waveform. These group-averaged waveforms were visually inspected across all scalp-sites, and the familiar components of the VEP were identified (Foxe & Simpson, 2002). This allowed for definition of the precise timing of a given component and delineation of the scalp-sites at which each component was of maximal amplitude. Evoked responses to these simple visual stimuli showed the typical sequence of VEP components (P1, N1, P2) over occipital sites. Following this procedure, three time-windows were identified for analysis corresponding to peak components over central-occipital (Oz), left occipital (PO7 and O1) and right occipital (O2 and PO8) sites: 90–110 ms, 130–150 ms and 160–180 ms.

Although the use of broadly defined component peaks is a good means of limiting the number of statistical tests that will be conducted, these components clearly represent the activity of many simultaneously active brain generators at any given moment (Foxe & Simpson, 2002). In order to provide a more complete picture of the mechanisms underlying visual adaptation, we also present the scalp topographic maps for the time period in which significant adaptation is observed and conduct a source modeling analysis (discussed below).

Primary analysis

Statistical analyses were performed using custom MATLAB scripts (Mathworks), the Fieldtrip toolbox for EEG analysis (Oostenveld *et al.*, 2011), EEGLAB (Delorme & Makeig, 2004) and the SPSS software package (SPSS). For the paired experiment (Experiment 1), a repeated-measures analysis of variance (ANOVA) with factors of stimulus order (S1, S2), ISI (200 ms, 300 ms) and scalp-site (PO7, O1, Oz, O2, PO8) was performed for each of the time periods of interest (2 × 2 × 5 ANOVA). For the block experiment (Experiment 2), a repeated-measures ANOVA with factors of ISI (200 ms, 300 ms, 550 ms, 1050 ms, 2550 ms) and scalp-site (occipital/parieto-occipital sites: PO7, O1, Oz, O2, PO8) was performed for each of the time periods of interest (5 × 5 ANOVA). Significant effects were then examined using protected *post hoc* contrasts. The Greenhouse–Geisser correction was used to adjust *F*-values and probabilities when sphericity was violated; the original degrees of freedom are presented for each analysis.

Source-localization

In order to examine the brain generators for representative short and long ISI conditions, the data from Experiment 2, which provided greater discrepancy between ISIs, was modeled using the *L*ocal *Au*to *R*egressive *A*verage inverse solution (LAURA; Gonzalez Andino *et al.*, 2001; Grave de Peralta Menendez *et al.*, 2001), as implemented in the CARTOOL software by Denis Brunet (brainmapping.unige.ch/cartool). The linear-distributed inverse solution is based on a realistic head model with 4024 solutions points equally distributed within the gray matter of the Montreal Neurological Institute's average brain. The LAURA method deals with multiple simultaneously active sources of *a priori* unknown location, and makes no assumptions regarding the number or location of active sources. It selects the source configuration that best mimics the biophysical behavior of the electrical field and produces a unique estimation of the current source density inside the brain. That is, the estimated activity at one point depends on the activity at neighboring points as described by electromagnetic laws (Grave de Peralta-Menendez & Gonzalez-Andino, 1998). Mean scalp topographies of the main periods of interest were down-sampled from the 168-channel montage to a 111-channel montage by means of a 3D-spline interpolation (Perrin *et al.*, 1987; Lopez *et al.*, 2011).

Source reconstruction was performed at two levels. First, we applied LAURA to VEP maps for the 300 ms and 2550 ms ISI conditions. Because there were minimal differences in the scalp topography for the 200 ms, 300 ms, 550 ms ISIs (Fig. 5), the 300 ms ISIs served as a representative for the 'shorter' ISIs. Additionally, the scalp topographies for the 1050 ms and 2550 ms ISIs were also very similar, and so the 2550 ms ISI served as a representative for the 'longer' ISIs. With this, we were able to visualize the brain generators for the signals recorded under these two different presentations.

Second, we performed statistical analyses in the source space to test for regions sensitive to adaptation effects (i.e. regions distinguishing between 'fast' and 'slow' presentation rates). These theoretically play a role in modulating the differences observed in

the VEPs across ISIs. To do so, we determined for each participant and each condition (300 ms ISI and 2550 ms ISI) at the three time periods of interest, the mean corresponding VEP map. The inverse solution was applied to each individual VEP map. The inverse solutions for the representative short and long ISIs were compared statistically (paired randomization tests), with subjects as a repeated measure. To correct for multiple comparisons we applied a Bonferroni correction (α/number of electrodes, 0.05/160 = 0.0003125), which decreases the chances of Type I errors (Grave de Peralta Menendez *et al.*, 2001).

Individual participant level analysis

In Experiment 2, in order to investigate the robustness of adaptation and the minimum number of sweeps required for statistical significance at the individual participant level, we conducted a non-parametric randomization procedure (Maris & Oostenveld, 2007). For each participant we compared the amplitude recorded under the 2500 ms ISI condition against each of the other ISI conditions (200, 300, 550, 1050 ms) at the midline (Oz) and lateral (O1 & O2) occipital site for each of the time periods of interest (90–110, 130–150, 160–180 ms). These scalp-sites were chosen for analysis as they demonstrated the largest activation and strongest modulation in the group-level statistics.

The observed difference between the 2550 ms ISI and the test ISI was compared with a reference distribution of differences that was derived by iteratively randomizing between the two original data sets (i.e. individual-subject VEP amplitudes for the 2550 ms and test ISI) 10 000 times. The number of epochs selected for the bootstrapping process was a subset of the total, which increased in steps of 10 from 30 epochs until statistical significance or the maximum number of sweeps was reached (Nolan *et al.*, 2012). A one-tailed threshold of $P < 0.05$ was used to define significance. The *P*-value for a randomization test was calculated from the proportion of values in the reference difference distribution that exceeded the observed difference (Fiebelkorn *et al.*, 2011).

Results

The checkerboard annulus evoked a VEP that exhibited a different morphology based on scalp-site. Amplitudes were greatest over central occipital scalp. At the midline site (Oz) the first major VEP component had a peak at approximately 110 ms (negative-going) and the next major component peaked at approximately 180 ms (positive-going). At the most proximal lateral sites (O1 and O2), the first major VEP component had a peak approximately 150 ms (negative-going) and the next major component peaked at about 250 ms (positive-going). At the more distal lateral sites (PO7 and PO8), the first major component had a peak at approximately 100 ms (positive-going) and the next major component peaked at approximately 160 ms.

Experiment 1: paired-presentation

Figure 2 shows the group-averaged VEP waveforms for the 200 ms (red) and 300 ms (blue) ISIs, with the three time periods of interest highlighted by the opaque vertical gray boxes. These waveforms contain both the VEP elicited by the first stimulus in a pair (S1) as well as the VEP to the second stimulus (S2) in the pair. The figure also displays the VEP waveform elicited by the 'catch' trials (black). This response should be entirely equivalent to the one evoked by the S1 stimulus. Also shown are the 'derived' waveforms for the S2 VEP, which isolate the responses to the S2 from the continued activity related to the S1. These waveforms were derived by subtracting the 'catch' from the composite S1–S2 VEP and then shifting the isolated S2 response back in time by the appropriate delay (red-dashed for the 200 ms and blue-dashed for the 300 ms ISI). These waveforms are shown for the five scalp-sites of interest (PO7, O1, Oz, O2, PO8) over occipital and parieto-occipital scalp regions (see Fig. S3A for an alternate depiction of these tuning parameters). Contrary to what was expected, S2 response amplitudes appear greater than those to the S1, and this is most prominent over midline and right occipital scalp.

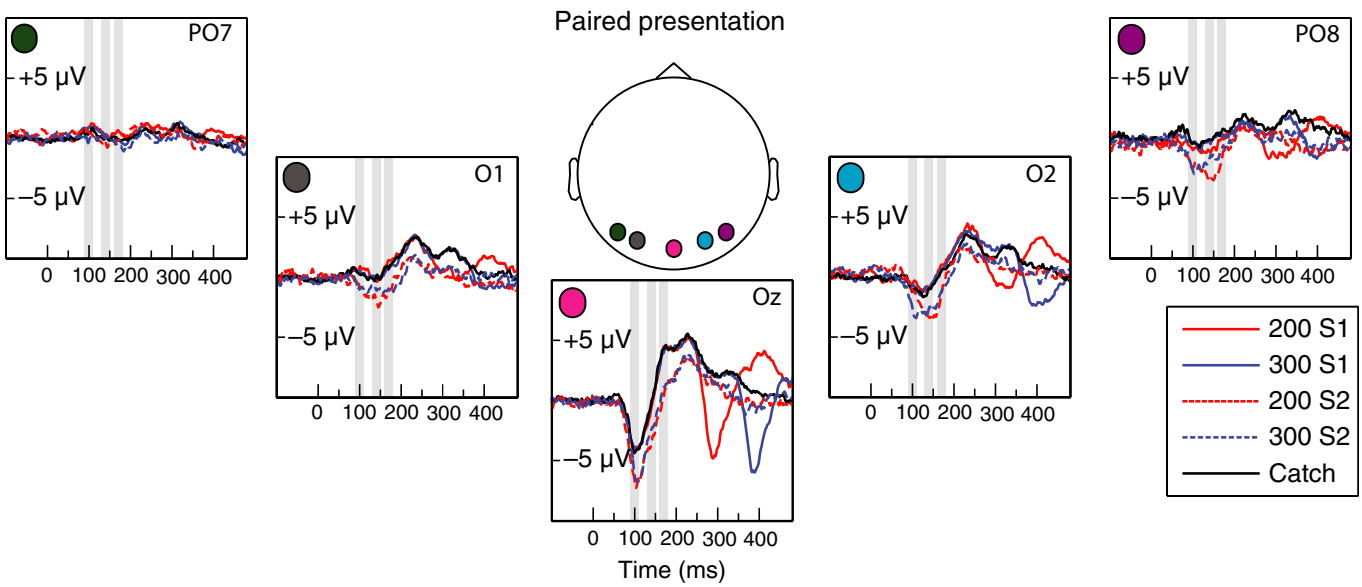

FIG. 2. Waveforms obtained from subtracting the catch trials from the 200 ms and 300 ms trials. The catch serves as the pure response to a single stimulus presentation (S1), and the trial waveform minus the catch represents the 'isolated' response to the second stimulus (S2). At 140 ms there is an effect of order, with VEPs to the S2 being greater than to the S1. At 170 ms, the effect reverses, with VEPs to the S2 being smaller (less positive) than to the S1. However, neither of these effects depends on ISI.

VEP amplitudes

Results from the three main ANOVAS performed to examine the effect of ISI, stimulus order, scalp-site and any interactions at each of the time periods of interest are presented in Table 1. In summary, the primary observation is a significant effect of order, with S2 VEP amplitudes larger than S1. This effect is primarily seen at lateral occipital sites for the two later time periods. This analysis captures the major negative-going peak in the VEP at these sites, spanning from 130 to 180 ms. At the midline site (Oz), this enhancement effect is seen during the first time-window of analysis, which at this site captures the peak of the major negative-going component (approximately 100 ms). The effect then reverses during the last time-window of analysis, with S2 amplitudes attenuated compared with S1. Here the analysis captures the peak of a major positive-going component in the VEP at 180 ms.

Scalp topographies

Scalp topographic maps representing interpolated potential distributions of the grand mean are shown for the catch trial, the 200 ms ISI and the 300 ms ISI conditions (columns), and the three periods of interest (rows) in Fig. 3. The first row of topographical distributions for the 90–110 ms period shows a strong central occipital distribution that is similar for both ISIs. The second row of topographical distributions for the 130–150 ms period shows evidence for a somewhat more bilateral occipital distribution, with greater amplitude evident over the right occipital scalp, and this activity shows clearly greater negativity for the S2 stimuli. The third row of topographical distributions for the 160–180 ms time period of interest shows a positive central occipital distribution with an evident decrease in amplitude to the S2 stimuli. Further, these maps show indistinguishable topographic distributions for the S1 and catch trials, providing further evidence that they are a representation of the same process.

Experiment 2: block-presentation

Figure 4A shows the group-averaged VEP waveforms for the five ISIs at the five targeted scalp-sites over occipital and parieto-occipital areas with the three time periods of interest highlighted by the vertical gray boxes. Figure 5B is a more focused representation of the effects of ISI on VEP at each scalp-site during the three time periods of interest. Together, these figures illustrate clear adaptation effects that vary as a function of ISI, scalp-site and time period of analysis. The most prominent effect is seen in the influence of ISI on the first major negative-going response, with a more negative-going response for longer ISI conditions. However, the midline occipital site also shows a second phase of adaptation, where a reversal of this effect is seen for the later major going positive component (see Fig. S3B for an alternate depiction of these tuning parameters, in which tuning functions are derived for each of the five scalp-sites using the group mean and standard error amplitude of the VEP for each ISI for the time periods of interest).

VEP amplitudes

Results from the three main ANOVAS performed to examine the effect of ISI, scalp-site and any interactions at the three time periods of interest (90–110 ms, 130–150 ms and 160–180 ms) are presented in Table 2. In summary, significant adaptation effects are noted at all sites examined, with the major finding being that VEP amplitudes decrease with faster ISIs. This robust effect is noted during the later time-windows, spanning 130–180 ms, for the lateral occipital sites. At these sites (PO7, O1, PO8, O2), this time-window captures the major negative-going component of the VEP. For the midline site (Oz), the adaptation effect is also noted at the first negative-going peak, which at this site occurs earlier and spans 110–140 ms. The effect at Oz then reverses during the last time-window of analysis, with VEP amplitudes increasing with faster ISIs. This time-window captures the major positive-going component at this site, which peaks at approximately 180 ms.

TABLE 1. Experiment 1 (A) Main ANOVA results summary for Experiment 1 (paired-presentation), (B) *Post hoc* comparisons for Experiment 1 (paired-paradigm)

	90–110 ms	130–150 ms	160–180 ms
(A) Experiment 1: paired-presentation			
ISI	n.s.	n.s.	n.s.
Order	$F_{1,10} = 17.725$, $P = 0.002$ S2 amplitude > S1 amplitude	$F_{1,10} = 19.859$, $P = 0.001$	$F_{1,10} = 13.609$, $P = 0.004$*
Scalp-site	$F_{4,40} = 7.997$, $P < 0.004$* Midline amplitudes > lateral amplitudes	$F_{4,40} = 2.692$, $P = 0.045$	$F_{4,40} = 4.554$, $P = 0.015$*
ISI × order	n.s.	n.s.	n.s.
ISI × scalp-site	n.s.	n.s.	n.s.
Order × scalp-site	n.s.	$F_{4,40} = 4.071$, $P = 0.007$ S2 amplitude > S1 amplitude, greatest differences at midline, lessens more laterally	$F_{4,40} = 5.038$, $P = 0.002$ S1 amplitude > S2 amplitude but only at midline, all other lateral sites S2 > S1
ISI × order × scalp-site	n.s.	n.s.	n.s.

Time scalp-site	PO7	O1	Oz	O2	PO8
(B) *Post hoc t*-tests					
90–110 ms	n.s.	*$t_{21} = 3.755$, $P = 0.001$*	*$t_{21} = 4.665$, $P < 0.001$*	n.s.	*$t_{21} = 3.879$, $P = 0.001$*
130–150 ms	n.s.	*$t_{21} = 2.957$, $P = 0.008$*	*$t_{21} = 8.525$, $P < 0.001$*	*$t_{21} = 4.479$, $P < 0.001$*	*$t_{21} = 4.004$, $P = 0.001$*
160–180 ms	n.s.	*$t_{21} = 3.828$, $P = 0.001$*	*$t_{21} = 7.294$, $P < 0.001$*	*$t_{21} = 3.862$, $P = 0.001$*	*$t_{21} = 2.959$, $P = 0.007$*

ISI, inter-stimulus interval.
Italics indicate a significant effect of ISI at that scalp-site.
Refer to Table 1A for interpreting the directionality of these effects.
*Indicates a Greenhouse-Geisser correction was applied.

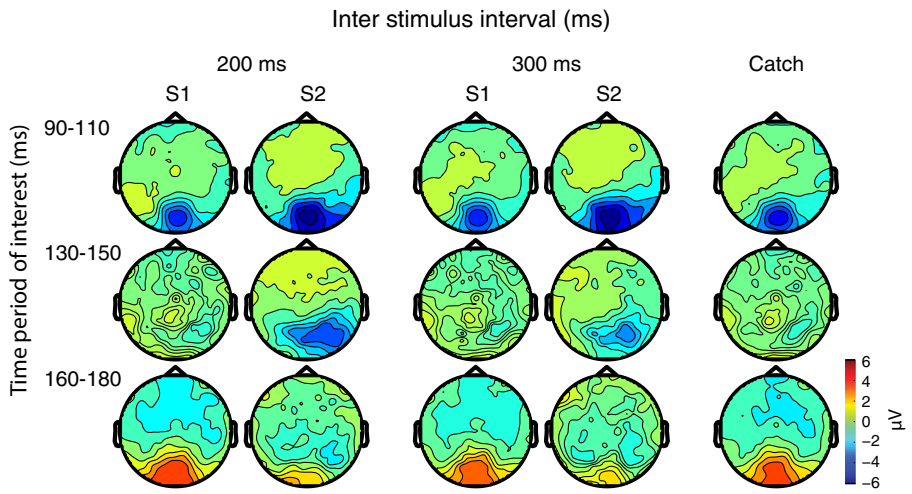

FIG. 3. Scalp topographic maps for the paired-paradigm reveal a difference between the first and second stimulus presentations and between the second and the catch for both inter-stimulus intervals (ISIs). Additionally there is a clear difference in topography when comparing the response at 100 ms and 140 ms (strong negativity) with the response at 170 ms (strong positivity).

TABLE 2. Experiment 2 (A) Main ANOVA results summary for Experiment 2 (block-presentation), (B) *Post hoc* comparisons for Experiment 2 (block-paradigm)

	90–110 ms	130–150 ms	160–180 ms
(A) Experiment 2: block-presentation			
ISI	n.s.	$F_{4,56}$ = 15.561, P < 0.001*	$F_{4,56}$ = 24.573, P < 0.0001*
Scalp-site	$F_{4,56}$ = 15.956, P < 0.001*	$F_{4,56}$ = 6.335, P = 0.003*	$F_{4,56}$ = 12.114, P < 0.0001*
ISI × scalp-site	$F_{16,224}$ = 3.400, P = 0.005*	$F_{16,224}$ = 7.175, P < 0.001*	$F_{16,224}$ = 6.817, P < 0.0001*
	Adaptation at midline and O1: faster ISIs = smaller VEPs	Adaptation strongest at midline, but seen everywhere: faster ISIs = smaller VEPs	Midline: slower ISIs = smaller VEPs All other lateral sites, faster ISIs = smaller VEPs

Time scalp-site	PO7	O1	Oz	O2	PO8
(B) Repeated-measures *post hoc* ANOVA					
90–110 ms	n.s.	*$F_{4,56}$ = 4.209, P = 0.024**	*$F_{4,56}$ = 4.957, P = 0.014**	n.s.	n.s.
130–150 ms	*$F_{4,56}$ = 6.083, P = 0.007**	*$F_{4,56}$ = 15.447, P < 0.001**	*$F_{4,56}$ = 20.017, P < 0.001**	*$F_{4,56}$ = 14.095, P < 0.001**	*$F_{4,56}$ = 4.656, P = 0.017**
160–180 ms	*$F_{4,56}$ = 8.906, P = 0.002**	*$F_{4,56}$ = 21.102, P < 0.001**	*$F_{4,56}$ = 30.012, P < 0.001**	*$F_{4,56}$ = 25.302, P < 0.001**	*$F_{4,56}$ = 10.062, P < 0.001**

ISI, inter-stimulus interval; VEP, visual-evoked potential.
Italics indicate a significant effect of ISI at that scalp-site. Refer to Table 2A for interpreting the directionality of these effects.
*Indicates a Greenhouse-Geisser correction was applied.

Scalp topographies

Scalp topographic maps representing interpolated potential distributions are shown of the group mean for all ISI conditions (columns) during the three time periods of interest (rows) in Fig. 5, right. The first row of topographical distributions for the 90–110 ms time period shows a stronger focal midline occipital distribution, which is similar for all ISIs in this time-window. The second row of topographical distributions for the 130–150 ms time period shows a progression of topographies with respect to the ISI, from a positive central occipital distribution for the shortest ISIs of 200 ms to a negative bilateral occipital distribution for the longer ISIs of 1050 ms and 2550 ms. The third row of topographical distributions for the 160–180 ms time period of interest shows a progression of topographies from a positive central occipital distribution for the shortest ISI (200 ms) to a negative bilateral occipital distribution for the longest ISI (2550 ms).

Difference topographies were also computed by comparing the interpolated potential distributions for the 2550 ms ISI condition against each of the other conditions (200 ms, 300 ms, 550 ms and 1050 ms ISIs) for the later time periods, which showed a significant effect of ISI on VEP amplitude (Fig. 5, left). The difference scalp topographic maps for the 90–110 ms timeframe (top row) show an emerging central negativity focus, with the strongest difference signal seen when comparing the two most discrepant ISIs (2550 vs. 200 ms), as can be seen here though differences in this time-window are weaker and also highly similar across ISIs. During the 130–150 ms timeframe (second row), difference maps reveal a strong central-occipital negativity that is similar across the comparisons between the 2550 ms ISI vs. the 200 ms, 300 ms and 550 ms ISI, but weaker between the most similar ISIs (1050 ms vs. 2550 ms), confirming a similar activation profile for the three shorter ISIs, but a difference between short and long ISIs. The 160–180 ms timeframe (bottom row) revealed a similar strong central-occipital negativity for each

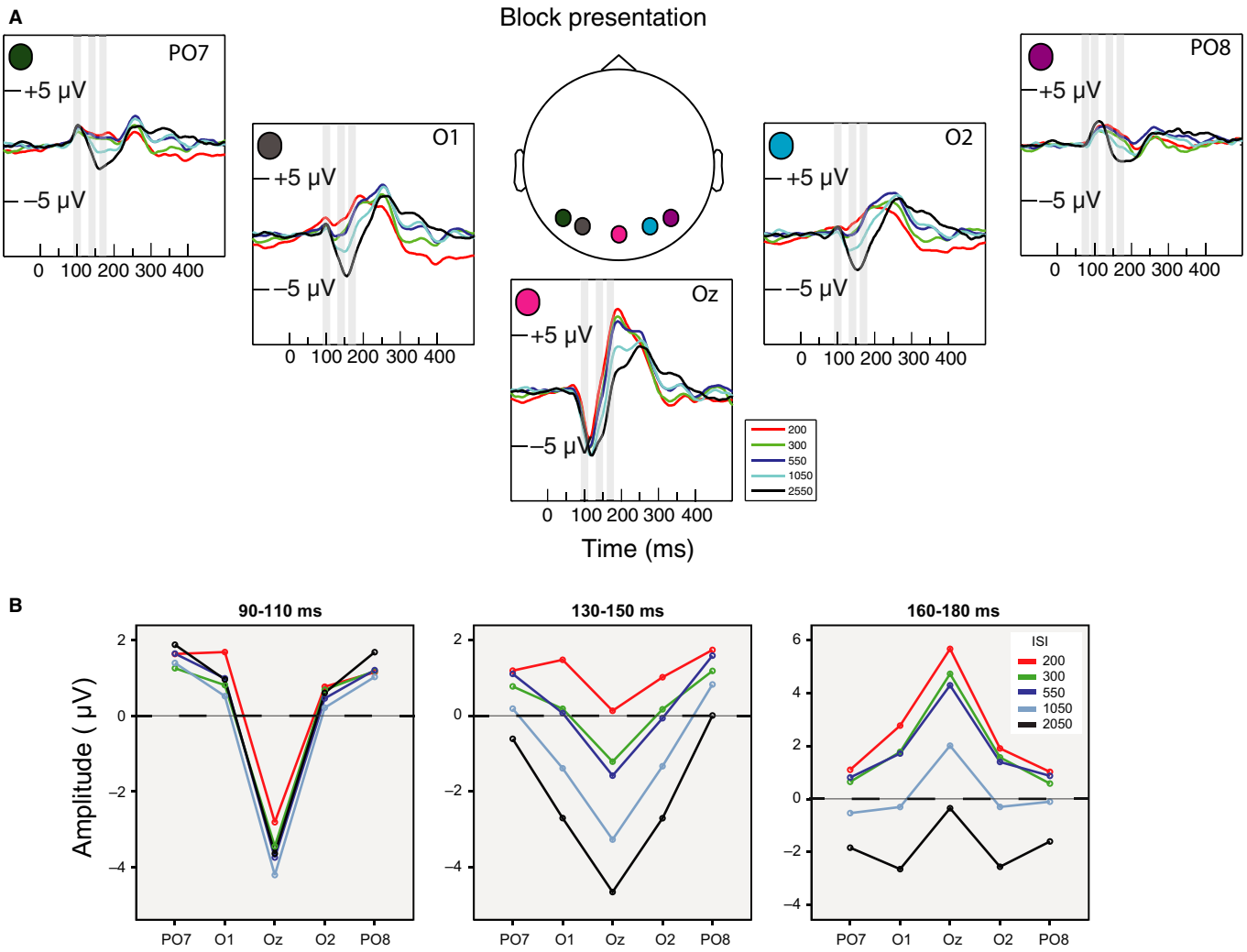

FIG. 4. (A) Average waveforms for each of the five ISI conditions (Experiment 2) are displayed for the five occipital and occipito-parietal scalp-sites of interest. A clear effect of ISI on VEP amplitude can be seen between 100 ms and 200 ms, with slower stimulus presentation rates leading to greater absolute VEP amplitude. (B) Amplitude by ISI plots. The effect of ISI on VEP amplitude at each scalp-site for the three time periods of interest. The greatest adaptation based on ISI is seen in the later time-windows (130–150 ms and 160–180 ms) and is most robust at the central occipital site. Additionally, the directionality of adaptation by ISI at the central site (Oz) is exclusively reversed in the last time period of interest, with the slowest ISI here eliciting the smallest VEP amplitudes.

comparison, which again was weakest for the 1050 ms vs. 2550 ms subtraction. In summary, the three shorter ISIs exhibit a response pattern that is different from the two longest ISIs but relatively similar to each other. The 1050 ms ISI response is unique as compared with the shorter ISIs, and is most similar to the 2550 ms condition, but still distinct. More modest differences in frontal activation are also noted in the topographic maps across time and ISI.

Source-localization

A source-localization model was applied to better understand the generators of the adaptation effects seen in this experiment for the time period during which there was sufficient signal strength in the waveforms and difference topographies (Fig. 6A). In the 90–110 ms interval (top row), the main brain generators were localized bilaterally to regions in and surrounding the occipital pole, pointing to striate and extrastriate generators in this timeframe for both the 300 ms and 2550 ms conditions. These sources encompassed parts of Brodmann area 17 (primary visual cortex), area 18 (parastriate visual association areas) and area 19 (extrastriate visual association areas). In the 130–150 ms interval (middle row), brain activation extended into extrastriate areas (relative to the 90–110 ms period), and included both dorsal and ventral visual regions (Brodmann 18 and 19). Additionally, the 2550 ms ISI condition contained generators located more dorsal/superior in comparison to the 350 ms ISI sources for this time period, but still including strong inferior occipital cortex activation. Additionally, there was minor activation of the middle temporal gyrus (including association areas in Brodmann 21 involved in object form and motion processing and temporal recognition) in the 2550 ms condition in this time period.

In the 160–180 ms time-window (bottom row), the main generators for both conditions localized to more inferior occipital regions as compared with the previous time period. In the 300 ms condition, sources were over Brodmann area 18 along with some activation over Brodmann area 7, which is part of the parietal cortex and involved in visuo-motor coordination. In the 2550 ms condition, there was inferior lateral activation involving the lingual gyrus and Brodmann area 19.

Randomization tests conducted to compare the signal sources identified above revealed significant differences between the two

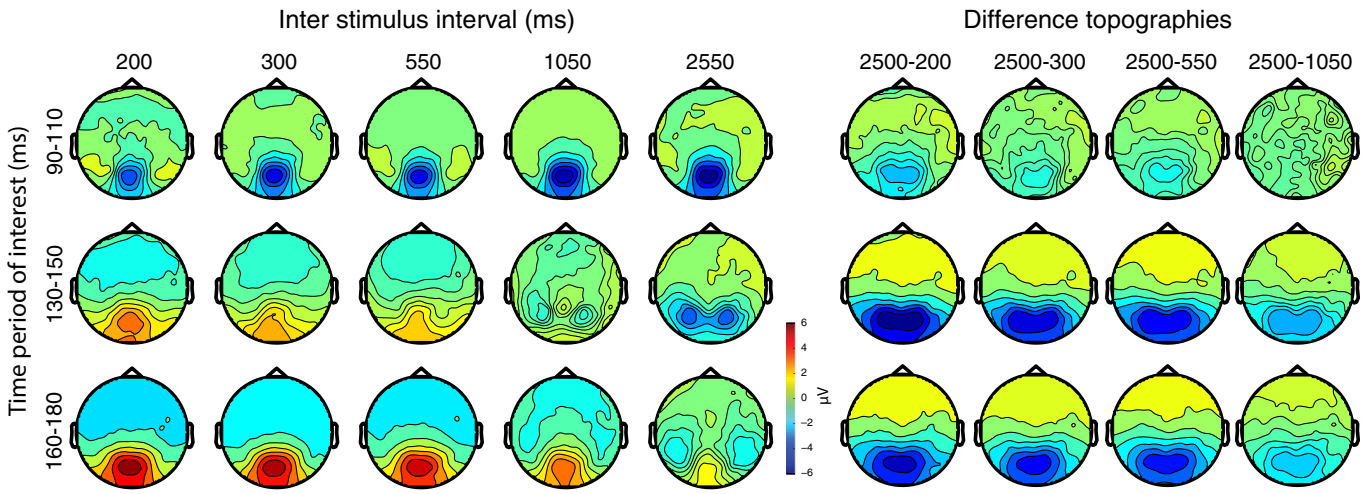

FIG. 5. (Left) Scalp topographic maps reveal similar central-occipital negativity for the early time period across inter-stimulus intervals (ISIs) in the block-presentation. At the later time points the voltage distribution diverges, with the shorter ISIs showing central-occipital positivity and the longer ISIs a bilateral negativity. (Right) Scalp topographic maps depicting the difference in electrical activation when comparing the 2550 ms condition with each of the other ISIs. The difference topography is most unique when comparing electrical activation across the scalp when comparing the 1050 ms ISI with the 2050 ms ISI at 140 ms and 180 ms post-stimulus presentation.

conditions for all three time periods, as can be seen in Fig. 6B. In the 90–110 ms time-window, the differences were localized to the occipital lobule, superior parietal lobule, lingual gyrus and medial frontal gyrus. Differences in the 130–150 ms time-window were most pronounced, spanning the middle temporal gyrus of the temporal lobe, the postcentral gyrus in the parietal lobe and the superior frontal gyrus encompassing Brodmann area 8, which is involved in motor planning and encompasses the frontal eye fields. The 160–180 ms time-window revealed the fewest significantly different sources across the two conditions. These were localized to frontal areas, including the middle frontal gyrus (Brodmann area 9) and the superior frontal gyrus.

Individual participant level analyses

We sought to establish how robust these measures of adaptation were and to assess whether significant adaptation functions could be observed consistently at the individual participant level, as a major

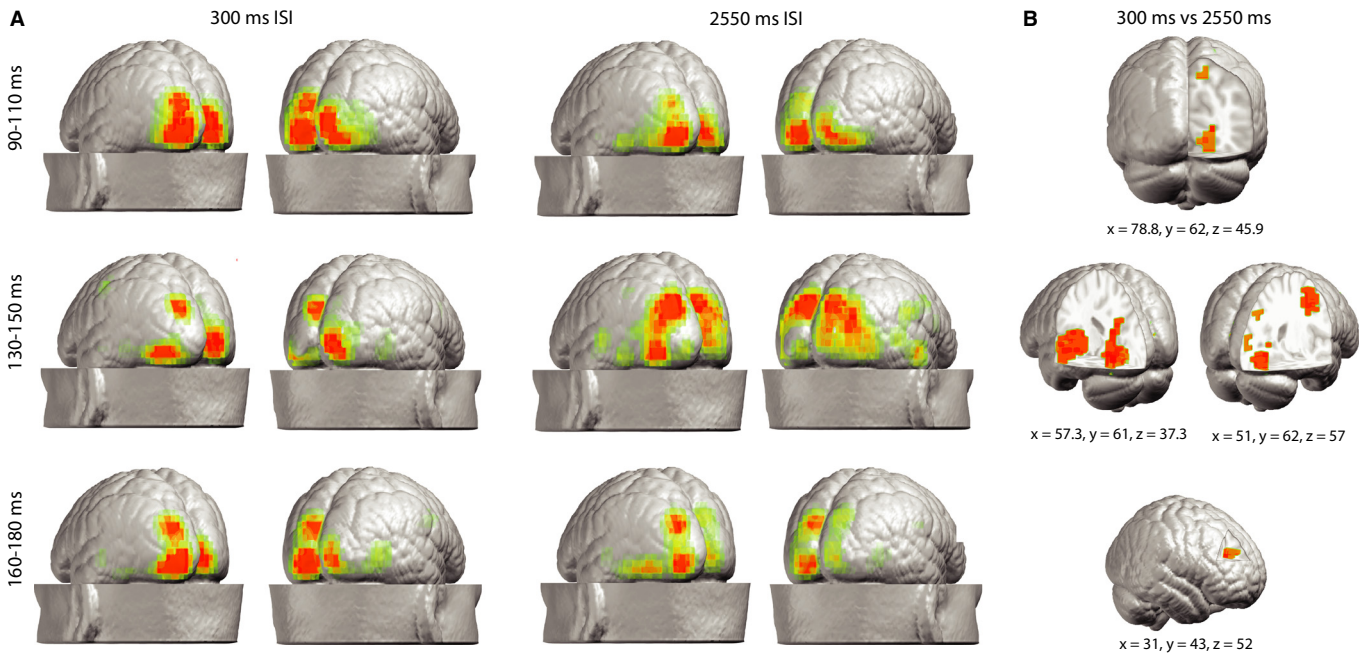

FIG. 6. (A) Brain generators estimated using a distributed linear inverse solution on the local auto regressive average (LAURA) for block-design. Early sources are mainly over the occipital cortex, with later sources extending over the parietal and temporal cortex. (B) Randomization tests reveal significant differences in brain generators between the 300 ms and 2550 ms conditions. At 90–110 ms these differences are mostly occipital. At 130–150 ms the differences are most pronounced and expand over occipital, parietal, temporal and frontal areas, including the superior parietal cortex and lateral occipital cortex. At 160–180 ms, the only significantly different sources are frontal. ISI, inter-stimulus interval.

aim here is to develop this measure as a potential biomarker of disease. If it is to serve as such, it will be imperative that it is robust at the individual level. Individual participant randomization analysis was conducted comparing the longest ISI (2550 ms) with each of the other ISIs (200 ms, 300 ms 550 ms, 1050 ms) at the three time periods of interest at the central occipital electrode site (Oz) and two lateral sites (O1 and O2). Table 3 shows the number of participants exhibiting significant adaptation effects along with the average and standard deviation of the number of sweeps required for this effect, as a function of ISI. Overall, participants showed significant differences in amplitude between the most discrepant ISIs (i.e. 200 ms, 300 ms and 550 ms vs. 2550 ms). For the middle time period of interest (130–150 ms), all participants showed significant differences between the shortest (200 ms ISI) and the longest (2550 ms ISI) at the central occipital site. The 160–180 ms time period contained the most stable effects across scalp-sites and ISIs. During this period, at least 14 of the 15 participants showed significant VEP amplitude differences for all of the ISI comparisons at Oz, all participants showed significant VEP differences for the two shorter ISIs (200 ms and 300 ms) against the 2550 ms ISI at Oz and O2, and 13 out of 15 at O1. The individual participant analysis results are in line with the group statistics, with the largest difference occurring at the later time periods.

Representative individual waveforms for three participants are depicted in Fig. 7. VEPs to a 'fast' ISI condition (300 ms) and 'slow' ISI condition (2550 ms) are plotted for the central occipital site and the two lateral sites. Amplitude values along these waveforms were taken for each individual subject to conduct the analysis described above. Here it can be seen that even at the individual level modulations based on presentation rate are evident. The dashed line in this figure represents the difference in amplitude between these two conditions (fast vs. slow) and can be interpreted as an index of adaptation.

Discussion

High-density VEPs were recorded in a pair of experiments to examine visual adaptation in healthy human adults as a function of presentation rate and of using a block- vs. a paired-presentation approach. In Experiment 1, stimuli were presented in pairs with relatively fast ISIs of 200 ms or 300 ms. In Experiment 2, stimuli were presented in much longer blocks (100 stimuli/block), while ISI was parametrically manipulated across blocks (ISIs of 200 ms, 300 ms, 550 ms, 1050 ms and 2550 ms, respectively). The data revealed clear evidence for adaptation during block-presentations, with dramatic and consistent modulation of VEP amplitude as a function of presentation rate. In contrast, the paired-stimulation approach resulted in more modest VEP amplitude changes and, despite the fact that similarly fast ISIs were employed as in the blocked experiment, there was no clear attenuation effect of the major VEP components across scalp-sites. In fact, the effects reported for Experiment 1 were opposite to what are classically expected using paired-adaptation paradigms, where the typical finding is a decrease in amplitude of the evoked response to the repeated stimulus during the earliest phases of processing. A second major goal of the current study was to establish whether visual adaptation functions could be reliably observed at the individual participant level. This goal was realized, establishing a potentially powerful biomarker of visual-sensory function for deployment in clinical populations. In what follows, we discuss the results of these experiments in further detail and their implications for future work.

Experiment 1: paired-presentation paradigm

While on first consideration a lack of reduced VEP amplitude to the S2 might seem surprising, a close examination of the paired-presentation auditory adaptation literature reveals a more nuanced picture. At

TABLE 3. Individual subject analysis

No. of subjects out of 15 (average minimum no. of sweeps required ± SD)				
2550 vs.	200	300	550	1050
(A) Central occipital site (Oz)				
90–110 ms	7 (66 ± 26)	8 (90 ± 58)	8 (93 ± 50)	3 (93.3 ± 31)
130–150 ms	15 (56 ± 27)	13 (57 ± 33)	13 (48 ± 14)	10 (60 ± 28)
160–180 ms	15 (57 ± 27)	15 (58 ± 35)	14 (49 ± 20)	14 (69 ± 40)
No. of subjects out of 15 (average minimum no. of sweeps required ± SD)				
2550 vs.	200	300	550	1050
(B) Right lateral site (O2)				
90–110 ms	8 (98 ± 61)	10 (114 ± 55)	12 (105 ± 58)	6 (136 ± 66)
130–150 ms	14 (50 ± 16)	13 (50 ± 14)	13 (62 ± 44)	12 (76 ± 30)
160–180 ms	15 (66 ± 34)	15 (66 ± 24)	14 (56 ± 17)	11 (90 ± 42)
No. of subjects out of 15 (average minimum no. of sweeps required ± SD)				
2550 vs.	200	300	550	1050
(C) Left lateral site (O1)				
90–110 ms	9 (72 ± 29)	9 (79 ± 34)	9 (95 ± 46)	8 (127.6 ± 54)
130–150 ms	13 (65 ± 41)	13 (69 ± 53)	13 (53 ± 19)	12 (75 ± 41)
160–180 ms	13 (68 ± 34)	13 (58 ± 19)	13 (55 ± 14)	10 (92 ± 54)

Results from randomization tests comparing the VEP at the central occipital site and two lateral sites for the 2550 ms condition against all other ISIs, for the three time periods of interest. Individual-level VEP modulation is seen in all participants in the 160–180 ms time period when comparing the most disparate ISIs for the central site and one lateral site.

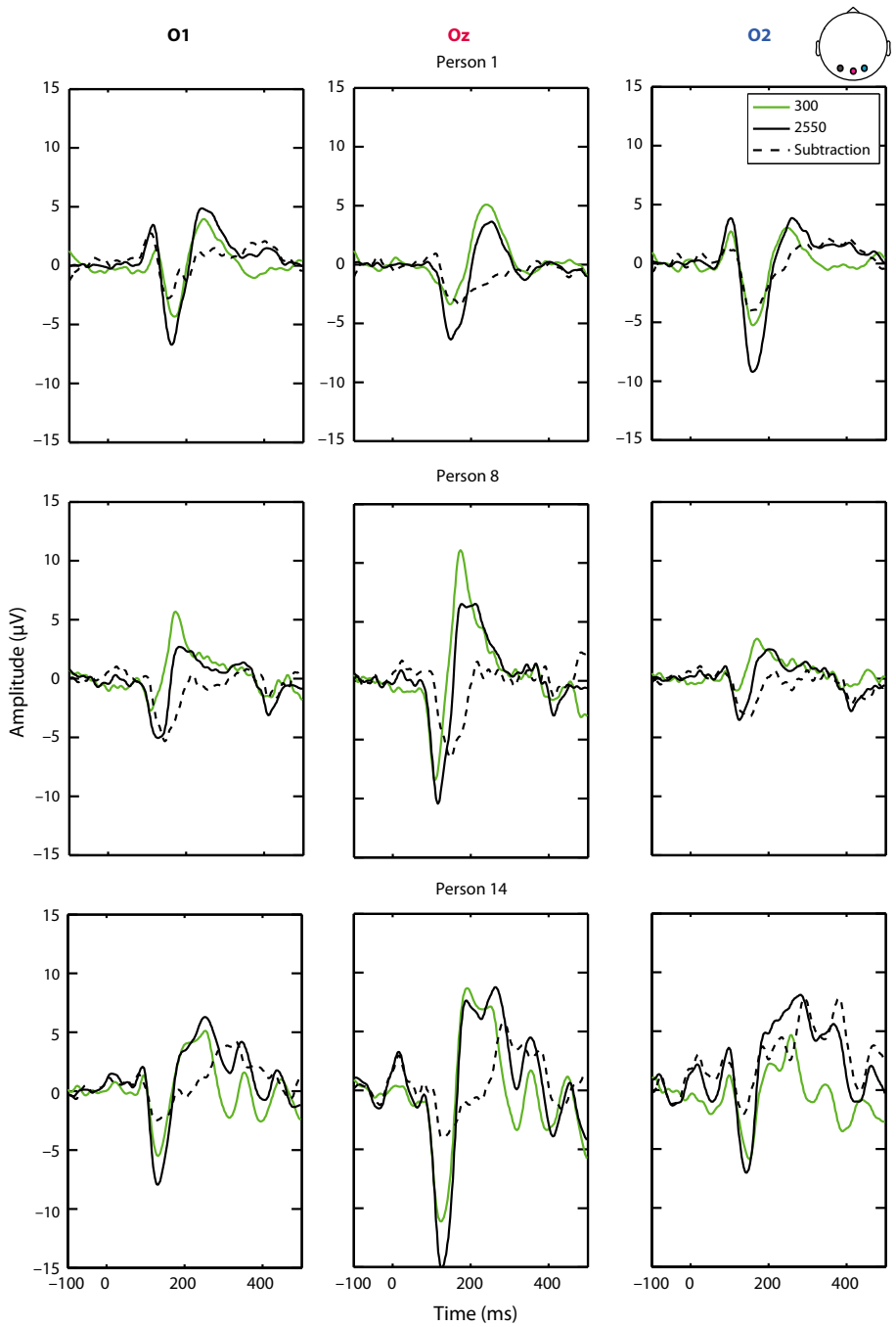

FIG. 7. Representative individual participant VEP waveforms. VEP to a 'fast' ISI condition (300 ms) and 'slow' ISI condition (2550 ms) is plotted for the central occipital site. The dashed line represents the difference in amplitude between these two conditions and can be interpreted as an index of adaptation.

ISIs in the range of those used here, response enhancement rather than suppression has sometimes been observed (Budd & Michie, 1994; Loveless *et al.*, 1996; Sable *et al.*, 2004; Wang *et al.*, 2008). For instance, Loveless and colleagues demonstrated that the classic P50 attenuation effect seen in the AEP can be reversed if ISIs < 400 ms are employed (Loveless *et al.*, 1989). This, however, is not always the case, with both auditory and visual responses also showing attenuation to even shorter ISIs (< 100 ms) during both early and late stages of processing (Gawne *et al.*, 2011). Alternatively, it is possible that certain short ISIs (40–90 ms) fall within the refractory period of human visual neurons, with observed attenuation occurring as a result of a decrease in the excitability of visual cortex and multiple stimuli being perceived as one (Musselwhite & Jeffreys, 1983; Skrandies & Raile, 1989; Coch *et al.*, 2005).

Another variable that may contribute to apparently contradictory results for the short ISI across paradigms is whether random or block-presentation of ISIs is employed. Here, the inter-pair interval randomly varied within the same block. Wang and colleagues have argued that S2 attenuation is seen only in blocks containing exclusively pairs of the same ISI (Wang *et al.*, 2010). Their reasoning is that only when the timing of the second stimulus is constant is it 'non-novel and highly predictable'(p. 2119), thereby eliciting a

reduced neural response. Thus, if ISI for each pair is variable within a block, S2 suppression may not be seen as timing is somewhat more unpredictable. Such an explanation could account for the lack of attenuation seen in Experiment 1 during the early time-windows of analysis. The later change from S2 enhancement to S2 attenuation as a result of processing stage reported here has also been previously observed in other sensory modalities (Wang *et al.*, 2008). Wang and colleagues in a paired, random ISI design, reported enhancement of the N1 wave and attenuation of the P2 wave for auditory and somatosensory stimuli when short ISIs were examined. Clearly, a greater range of ISIs and comparison of random vs. blocked ISI rate will be necessary to fully characterize these functions in the visual system.

Experiment 2: block-presentation paradigm

Comparable to what has been reported in the auditory and somatosensory literatures (Hämäläinen *et al.*, 1990; Pereira *et al.*, 2014), event-related potential (ERP) attenuation to repetitive stimulation, which was modulated by presentation rate, was observed. In Experiment 2, VEP attenuation was modulated by ISI, with faster presentation rates leading to smaller VEP amplitudes. Source analyses pointed to adaptation effects not only in early striate and extrastriate visual cortical areas, but also across a widespread network of higher order dorsal and ventral visual regions that extended into the frontal cortex. Further, the most robust adaptation effects in the visual system occurred some 65–100 ms after initial response onset (Foxe & Simpson, 2002), suggesting a more complex neurophysiological profile than previously assumed.

Whereas most ERP characterizations are conducted at the group level, a central aim of the current study was to quantify the individual subject reliability of these effects with the goal of developing a metric of visual processing that might prove useful as a biomarker. In the block-presentation paradigm (Experiment 2) the ISI-specific effects were measurable at both the group and individual level, most reliably seen starting at about 130 ms (in 15 out of 15 participants), whereas for the paired-presentation paradigm (Experiment 1) only the group effects were significant.

Very few studies have comprehensively examined the effect of multiple ISIs (presentation rates) on sensory adaptation in the visual system. This is perhaps because the wide variety of presentation paradigms utilized in the study of adaptation has made it difficult to elucidate a clear effect of stimulus repetition on the VEP amplitude. Here we find that a block-paradigm such as that used in Experiment 2 is well suited for investigations of short-term visual adaptation. Our data establish that adaptive filtering of repetitive visual stimulation is reliably characterized by: (1) challenging the visual system with increased repetition; and (2) thoroughly probing across stages of visual processing and scalp-sites. In contrast, the short-term plasticity mechanisms assayed in Experiment 2 are not adequately engaged in the paired-paradigm (Experiment 1).

The analysis approach presented in this paper provides a composite measure of overall adaptation across an entire block (i.e. a period of 100 stimuli) and compares this adaptation 'between' the various ISIs. However, the question as to when during the 100 stimuli in a given block the adaptation function stabilizes is one that our study was not designed to address (i.e. 'within' block adaptation). Taken together, the results from Experiments 1 and 2 suggest that certainly more than two trials are needed for adaptation to equilibrate. *Post hoc* analysis of the data from Experiment 2 indicate that it might be possible to adequately represent adaptation with sequences much shorter than 100 stimuli – likely in the range of 10 stimuli per train (Fig. S4). Thus, a shorter version of the experiment run on considerably greater numbers of individuals would allow for a much finer titration of the temporal course of adaptation in trains of stimuli, while contributing to 'normative data' against which clinical populations may be assessed, a matter for future work.

Lastly, source-localizations of the effects uncovered during the block experiment provide clues as to the potential mechanisms involved in this form of short-term sensory plasticity. It is noteworthy for instance that the adaptation effects uncovered here were not restricted to early striate and extrastriate regions, as one might initially expect with such a basic sensory assay. Rather, sources well beyond V1/V2 were differentially impacted by the varying presentation rates, including regions in both the dorsal and ventral streams, suggesting that adaptation impacts processing in regions within both the superior parietal cortex and the lateral occipital complex. It is perhaps surprising that adaptation should be seen in these higher-order regions for the simple stimuli used, especially because the stimuli were not task-relevant and were essentially ignored by the participants. Studies employing task-relevant stimuli, examining orientation adaptation, have also found response modulation in areas beyond V1 in both human (Fang *et al.*, 2005; Brunet *et al.*, 2014) and non-human participants (Hudson *et al.*, 2009; Wang *et al.*, 2011). In these, changes in neuronal synchronization, both local and between regions, have been implicated in the main findings. Understanding the role and mechanisms underlying the involvement of higher-order regions in the current adaptation paradigm is an important matter for future work.

Future directions

It is clear that the mechanistic and molecular underpinnings of basic adaptation are not yet fully understood. These mechanisms might differ between sensory modalities, taking into account inherent differences in disparate neuronal populations such as response, recovery and sampling rates. Studies employing pharmacological manipulations and measuring changes under both the paired-presentation and the block-presentation paradigms along with studies using the same paradigms across different sensory modalities may reveal whether the adaptation profile is consistent across paradigms and whether sensory adaptation dynamics are modality-specific.

A more complete understanding of sensory adaptation may follow from pharmacological studies targeting neurotransmitter systems implicated in adaptation. Studies assessing molecular mechanisms of adaptation in the auditory system are sparse and provide varying findings. There are reports of serotoninergic (Oranje *et al.*, 2011), dopaminergic (Light *et al.*, 1999) and nicotinergic effects (Knott *et al.*, 2010) on auditory adaptation. In the visual system, one group conducted an experiment in which light deprivation, which according to the authors downregulates the GABA-ergic system, lead to adaptation impairments (Palermo *et al.*, 2011). These impairments were reversed with exposure to high-frequency repeated transcranial magnetic stimulation, which had previously been shown to reverse light deprivation inhibitory effects.

An additional research question concerns the effects of attention on sensory adaptation. Recent studies have attempted to examine this interaction and, although the findings are still equivocal, there is some evidence for attention-modulated auditory adaptation (Rosburg *et al.*, 2009; Gjini *et al.*, 2011). This is of particular interest for both the characterization of adaptation in the general population, and in clinical groups, particularly those with documented attention deficits (i.e. schizophrenia, autism, etc.).

A primary motivation for the current study was to examine whether visual adaptation to varying presentation rates would be

used to elicit a robust metric of short-term visual plasticity, one that could ultimately be deployed as a sensitive assay of visual function in clinical populations. Our interest was specifically whetted by the fact that abnormal sensory adaptation functions have been repeatedly demonstrated in patients with schizophrenia, but these have been assayed almost exclusively using auditory stimulation (Patterson *et al.*, 2008; Olincy *et al.*, 2010), although there is emerging evidence for related deficits in the somatosensory system (Thoma *et al.*, 2007). Auditory adaptation deficits represent potentially powerful biomarkers of schizophrenia as they are also seen in a significant proportion of unaffected first-degree biological relatives of patients (Olincy *et al.*, 2010). In a series of experiments, we have shown that visual-sensory processing deficits are particularly robust in patients with schizophrenia (Foxe *et al.*, 2001, 2005; Doniger *et al.*, 2002; Lalor *et al.*, 2008, 2012; Yeap *et al.*, 2008a), a finding that has been observed across multiple labs (Mukundan, 1986; Spencer *et al.*, 2004; Haenschel *et al.*, 2007). Crucially, these deficits are also seen in first-degree relatives (Yeap *et al.*, 2006), first-episode drug-naïve patients (Yeap *et al.*, 2008b) and in young adults with high schizotypy (Koychev *et al.*, 2010; Bedwell *et al.*, 2013), pointing to their potential utility as risk endophenotypes (Gottesman & Gould, 2003; Magno *et al.*, 2008; Foxe *et al.*, 2011).

A drawback of many of these studies, however, is that despite between-group effect sizes that are typically large, intrinsic inter-individual variability in the amplitude and morphology of the VEP response reduces their effectiveness as potential classifiers. We have made the argument that one way to surmount this issue of inter-individual variance is to assay second-order dynamic effects of sensory systems such as short-term plasticity, as with the visual adaptation paradigm at hand. It is of note that dysfunctional sensory plasticity has recently been shown in patients with schizophrenia (Cavuş *et al.*, 2012; Foxe *et al.*, 2013). Of course, if any given metric of sensory processing is ultimately to serve as a diagnostically meaningful biomarker, it must be possible to assay it robustly at the individual patient level, and it is very encouraging that this is precisely what was found here for block-presentation paradigm. Thus, if short-term sensory plasticity is impaired in patients with schizophrenia, mapping visual adaptation functions such as those detailed here may yet prove a very powerful method of assaying said dysfunction.

Conclusions

Adaptation of brain responses to repetitive stimulation is considered a fundamental property of sensory processing. Here we employed high-density EEG in two variants of an adaptation design, examining the effect of presentation rate on VEP attenuation in a paired-paradigm and a block-paradigm. Robust VEP modulations were evident as a function of presentation rate in the block-paradigm, with the strongest modulations seen in the 130–150 ms and 160–180 ms phases of visual processing. In the paired design, we observed a more modest enhancement effect, with VEP amplitudes increasing when comparing S2 with S1. In order to better characterize the spatial and temporal properties of visual adaptation, we used the full set of information collected from our high-density array to create scalp topographic maps and model the neural generators of adaptation across time. These analyses revealed sources in striate, extrastriate and higher-order (e.g. superior temporal and lateral occipital) cortex. Importantly, in the block-paradigm, adaptation effects were statistically robust at the individual participant level. These results suggest that a taxing paradigm, such as the current block-paradigm, is better suited to engage adaptation mechanisms in the visual system compared with a paired design. The increased sensitivity of the visual processing metric obtained in the block-paradigm has implications for the examination of visual processing deficits in clinical populations.

Supporting Information

Additional supporting information can be found in the online version of this article:

Fig. S1. Catch trial subtraction for paired-presentation. VEP to the single stimulus is subtracted from the convoluted waveform containing both the VEP to the S1 and S2 stimuli (presented as a pair), resulting in the VEP elicited by the S2 alone.

Fig. S2. Adjacent response (ADJAR) algorithm for block-presentation was performed on subject-level data to model and remove any response overlap between short ISI stimuli.

Fig. S3. (A) Adaptation functions at the occipital and occipito-parietal electrode sites of interest across the three phases of processing in the paired-presentation paradigm. This highlights the order effect, with very little influence of ISI on adaptation for the two presentation rates examined. (B) Adaptation functions for the occipital and occipito-parietal electrode sites of interest across the three phases of processing in the block-presentation paradigm. These were derived by fitting an exponential decay function to the mean VEP amplitude across the five ISIs, for each site, at the specified time periods. This procedure yields a plot that can describe the data using three parameters: two constants (maximum and minimum values for amplitudes) and power (rate decay across ISIs).

Fig. S4. Adaptation across trials. The data matrix was progressively split into ever-finer sequential temporal bins in order to examine adaptation across a block of 100 stimuli. Four of these divisions are illustrated. There are a maximum of eight trials contributed by each individual per bin when the data are split into 24. It is evident here that adaptation is wholly similar across all bins and that it likely kicks in after just a handful of trials, which we simply do not have the signal-to-noise resolution to address in greater detail.

Acknowledgements

This study was supported by a grant from the US National Institute of Mental Health (NIMH) to J.J.F. and S.M. (RO1 - MH085322). The authors would like to express their gratitude to Ms Sarah Ruberman and Mr Frantzy Acluche for their many hours of work in support of this study. The Human Clinical Phenotyping Core, where the participants enrolled in this study were recruited and evaluated, is a facility of the Rose F. Kennedy Intellectual and Developmental Disabilities Research Center (RFK-IDDRC), which is funded by a center grant from the Eunice Kennedy Shriver National Institute of Child Health & Human Development (NICHD P30 HD071593). Ongoing support of The Cognitive Neurophysiology Laboratory is provided through a grant from the Sheryl and Daniel R. Tishman Charitable Foundation.

Conflict of interest statement

All authors of this paper declare no conflicts of interest, financial or otherwise, that could have biased their contributions to this work. The senior author, Dr Foxe, attests that all authors had access to the full dataset and to all stages of the analyses.

Abbreviations

ADJAR, adjacent response; AEP, auditory-evoked potential; EEG, electroencephalography; ERP, event-related potential; GABA, γ-aminobutyric acid; ISI, inter-stimulus interval; LAURA, Local Auto Regressive Average; VEP, visual-evoked potential.

References

Adler, L.E., Waldo, M.C. & Freedman, R. (1985) Neurophysiologic studies of sensory gating in schizophrenia: comparison of auditory and visual responses. *Biol. Psychiat.*, **20**, 1284–1296.

Arnfred, S.M., Eder, D.N., Hemmingsen, R.P., Glenthøj, B.Y. & Chen, A.C. (2001) Gating of the vertex somatosensory and auditory evoked potential P50 and the correlation to skin conductance orienting response in healthy men. *Psychiat. Res.*, **101**, 221–235.

Bedwell, J.S., Chan, C.C., Trachik, B.J. & Rassovsky, Y. (2013) Changes in the visual-evoked P1 potential as a function of schizotypy and background color in healthy young adults. *J. Psychiatr. Res.*, **47**, 542–547.

Braff, D.L., Light, G.A. & Swerdlow, N.R. (2007) Prepulse inhibition and P50 suppression are both deficient but not correlated in schizophrenia patients. *Biol. Psychiat.*, **61**, 1204–1207.

Brockhaus-Dumke, A., Mueller, R., Faigle, U. & Klosterkoetter, J. (2008) Sensory gating revisited: Relation between brain oscillations and auditory evoked potentials in schizophrenia. *Schizophr. Res.*, **99**, 238–249.

Brunet, N.M., Bosman, C.A., Vinck, M., Roberts, M., Oostenveld, R., Desimone, R., De Weerd, P. & Fries, P. (2014) Stimulus repetition modulates gamma-band synchronization in primate visual cortex. *Proc. Natl. Acad. Sci. USA*, **111**, 3626–3631.

Budd, T.W. & Michie, P.T. (1994) Facilitation of the N1 peak of the auditory Erp at short stimulus intervals. *NeuroReport*, **5**, 2513–2516.

Budd, T.W., Barry, R.J., Gordon, E., Rennie, C. & Michie, P.T. (1998) Decrement of the N1 auditory event-related potential with stimulus repetition: habituation vs. refractoriness. *Int. J. Psychophysiol.*, **31**, 51–68.

Butler, J.S., Molholm, S., Fiebelkorn, I.C., Mercier, M.R., Schwartz, T.H. & Foxe, J.J. (2011) Common or redundant neural circuits for duration processing across audition and touch. *J. Neurosci.*, **31**, 3400–3406.

Carlén, M., Meletis, K., Siegle, J.H., Cardin, J.A., Futai, K., Vierling-Claassen, D., Rühlmann, C., Jones, S.R., Deisseroth, K., Sheng, M., Moore, C.I. & Tsai, L.H. (2012) A critical role for NMDA receptors in parvalbumin interneurons for gamma rhythm induction and behavior. *Mol. Psychiatr.*, **17**, 537–548.

Cattan, S., Bachatene, L., Bharmauria, V., Jeyabalaratnam, J., Milleret, C. & Molotchnikoff, S. (2014) Comparative analysis of orientation maps in areas 17 and 18 of the cat primary visual cortex following adaptation. *Eur. J. Neurosci.*, **40**, 2554–2563.

Cavuş, I., Reinhart, R.M., Roach, B.J., Gueorguieva, R., Teyler, T.J., Clapp, W.C., Ford, J.M., Krystal, J.H. & Mathalon, D.H. (2012) Impaired visual cortical plasticity in schizophrenia. *Biol. Psychiat.*, **71**, 512–520.

Chang, W.P., Arfken, C.L., Sangal, M.P. & Boutros, N.N. (2011) Probing the relative contribution of the first and second responses to sensory gating indices: a meta-analysis. *Psychophysiology*, **48**, 980–992.

Chung, S., Li, X. & Nelson, S.B. (2002) Short-term depression at thalamocortical synapses contributes to rapid adaptation of cortical sensory responses in vivo. *Neuron*, **34**, 437–446.

Coch, D., Skendzel, W., & Neville, H.J. (2005) Auditory and visual refractory period effects in children and adults: an ERP study. *Clin. Neurophysiol.*, **116**, 2184–2203.

Davis, H., Osterhammel, P.A., Wier, C.C. & Gjerdingen, D.B. (1972) Slow vertex potentials: interactions among auditory, tactile, electric and visual stimuli. *Electroen. Clin. Neuro.*, **33**, 537–545.

Delorme, A. & Makeig, S. (2004) EEGLAB: an open source toolbox for analysis of single-trial EEG dynamics including independent component analysis. *J. Neurosci. Meth.*, **134**, 9–21.

Doniger, G.M., Foxe, J.J., Murray, M.M., Higgins, B.A. & Javitt, D.C. (2002) Impaired visual object recognition and dorsal/ventral stream interaction in schizophrenia. *Arch. Gen. Psychiat.*, **59**, 1011–1020.

Fang, F., Murray, S.O., Kersten, D. & He, S. (2005) Orientation-tuned FMRI adaptation in human visual cortex. *J. Neurophysiol.*, **94**, 4188–4195.

Fiebelkorn, I.C., Foxe, J.J., Butler, J.S., Mercier, M.R., Snyder, A.C. & Molholm, S. (2011) Ready, set, reset: stimulus-locked periodicity in behavioral performance demonstrates the consequences of cross-sensory phase reset. *J. Neurosci.*, **31**, 9971–9981.

Fiebelkorn, I.C., Foxe, J.J., McCourt, M.E., Dumas, K.N. & Molholm, S. (2013) Atypical category processing and hemispheric asymmetries in high-functioning children with autism: revealed through high-density EEG mapping. *Cortex*, **49**, 1259–1267.

Foxe, J.J. & Simpson, G.V. (2002) Flow of activation from V1 to frontal cortex in humans. A framework for defining "early" visual processing. *Exp. Brain Res.*, **142**, 139–150.

Foxe, J.J., Doniger, G.M. & Javitt, D.C. (2001) Early visual processing deficits in schizophrenia: impaired P1 generation revealed by high-density electrical mapping. *NeuroReport*, **12**, 3815–3820.

Foxe, J.J., Murray, M.M. & Javitt, D.C. (2005) Filling-in in schizophrenia: a high-density electrical mapping and source-analysis investigation of illusory contour processing. *Cereb. Cortex*, **15**, 1914–1927.

Foxe, J.J., Yeap, S., Snyder, A.C., Kelly, S.P., Thakore, J.H. & Molholm, S. (2011) The N1 auditory evoked potential component as an endophenotype for schizophrenia: high-density electrical mapping in clinically unaffected first-degree relatives, first-episode, and chronic schizophrenia patients. *Eur. Arch. Psy. Clin. N.*, **261**, 331–339.

Foxe, J.J., Yeap, S. & Leavitt, V.M. (2013) Brief monocular deprivation as an assay of short-term visual sensory plasticity in schizophrenia – "the binocular effect". *Front. Psychiatr.*, **4**, 164.

Frey, H.P., Molholm, S., Lalor, E.C., Russo, N.N. & Foxe, J.J. (2013) Atypical cortical representation of peripheral visual space in children with an autism spectrum disorder. *Eur. J. Neurosci.*, **38**, 2125–2138.

Friston, K. (2005) A theory of cortical responses. *Philos. T. Roy. Soc. Lond. B.*, **360**, 815–836.

Fruhstorfer, H., Soveri, P. & Järvilehto, T. (1970) Short-term habituation of the auditory evoked response in man. *Electroen. Clin. Neuro.*, **28**, 153–161.

Gawne, T.J., Osbourne, T.S. & Risner, M.L. (2011) Robust sensory gating in the cortical visual evoked potential using two spatially separated stimuli. *Clin. Neurophysiol.*, **122**, 588–593.

Gjini, K., Sundaresan, K. & Boutros, N.N. (2008) Electroencephalographic evidence of sensory gating in the occipital visual cortex. *NeuroReport*, **19**, 1519–1522.

Gjini, K., Burroughs, S. & Boutros, N.N. (2011) Relevance of attention in auditory sensory gating paradigms in schizophrenia A pilot study. *J. Psychophysiol.*, **25**, 60–66.

Gonzalez Andino, S.L., Grave de Peralta Menendez, R., Lantz, C.M., Blank, O., Michel, C.M. & Landis, T. (2001) Non-stationary distributed source approximation: an alternative to improve localization procedures. *Hum. Brain Mapp.*, **14**, 81–95.

Gottesman, I.I. & Gould, T.D. (2003) The endophenotype concept in psychiatry: etymology and strategic intentions. *Am. J. Psychiat.*, **160**, 636–645.

Grave de Peralta-Menendez, R. & Gonzalez-Andino, S.L. (1998) A critical analysis of linear inverse solutions to the neuroelectromagnetic inverse problem. *IEEE T. Bio-med. Eng.*, **45**, 440–448.

Grave de Peralta Menendez, R., Gonzalez Andino, S., Lantz, G., Michel, C.M. & Landis, T. (2001) Noninvasive localization of electromagnetic epileptic activity. I. Method descriptions and simulations. *Brain Topogr.*, **14**, 131–137.

Grill-Spector, K., Henson, R. & Martin, A. (2006) Repetition and the brain: neural models of stimulus-specific effects. *Trends Cogn. Sci.*, **10**, 14–23.

Grzeschik, R., Böckmann-Barthel, M., Mühler, R., Verhey, J.L. & Hoffmann, M.B. (2013) Direction-specific adaptation of motion-onset auditory evoked potentials. *Eur. J. Neurosci.*, **38**, 2557–2565.

Haenschel, C., Bittner, R.A., Haertling, F., Rotarska-Jagiela, A., Maurer, K., Singer, W. & Linden, D.E. (2007) Contribution of impaired early-stage visual processing to working memory dysfunction in adolescents with schizophrenia: a study with event-related potentials and functional magnetic resonance imaging. *Arch. Gen. Psychiat.*, **64**, 1229–1240.

Hämäläinen, H., Kekoni, J., Sams, M., Reinikainen, K. & Näätänen, R. (1990) Human somatosensory evoked potentials to mechanical pulses and vibration: contributions of SI and SII somatosensory cortices to P50 and P100 components. *Electroen. Clin. Neuro.*, **75**, 13–21.

Hetrick, W.P., Sandman, C.A., Bunney, W.E. Jr., Jin, Y., Potkin, S.G. & White, M.H. (1996) Gender differences in gating of the auditory evoked potential in normal subjects. *Biol. Psychiat.*, **39**, 51–58.

Hudson, A.E., Schiff, N.D., Victor, J.D. & Purpura, K.P. (2009) Attentional modulation of adaptation in V4. *Eur. J. Neurosci.*, **30**, 151–171.

Knott, V.J., Fisher, D.J., & Millar, A.M. (2010) Differential effects of nicotine on P50 amplitude, its gating, and their neural sources in low and high suppressors. *Neuroscience*, **170**, 816–826.

Koychev, I., El-Deredy, W., Haenschel, C. & Deakin, J.F. (2010) Visual information processing deficits as biomarkers of vulnerability to schizophrenia: an event-related potential study in schizotypy. *Neuropsychologia*, **48**, 2205–2214.

Lalor, E.C., Yeap, S., Reilly, R.B., Pearlmutter, B.A. & Foxe, J.J. (2008) Dissecting the cellular contributions to early visual sensory processing deficits in schizophrenia using the VESPA evoked response. *Schizophr. Res.*, **98**, 256–264.

Lalor, E.C., De Sanctis, P., Krakowski, M.I. & Foxe, J.J. (2012) Visual sensory processing deficits in schizophrenia: is there anything to the magnocellular account? *Schizophr. Res.*, **139**, 246–252.
Lanting, C.P., Briley, P.M., Sumner, C.J. & Krumbholz, K. (2013) Mechanisms of adaptation in human auditory cortex. *J. Neurophysiol.*, **110**, 973–983.
Light, G.A., Malaspina, D., Geyer, M.A., Luber, B.M., Coleman, E.A., Sackeim, H.A. & Braff, D.L. (1999) Amphetamine disrupts P50 suppression in normal subjects. *Biol. Psychiat.*, **46**, 990–996.
Lopez, C., Mercier, M.R., Halje, P. & Blanke, O. (2011) Spatiotemporal dynamics of visual vertical judgments: early and late brain mechanisms as revealed by high-density electrical neuroimaging. *Neuroscience*, **181**, 134–149.
Loveless, N., Hari, R., Hämäläinen, M. & Tiihonen, J. (1989) Evoked responses of human auditory-cortex may be enhanced by preceding stimuli. *Electroen. Clin. Neuro.*, **74**, 217–227.
Loveless, N., Levänen, S., Jousmäki, V., Sams, M. & Hari, R. (1996) Temporal integration in auditory sensory memory: neuromagnetic evidence. *Electroen. Clin. Neuro.*, **100**, 220–228.
Magno, E., Yeap, S., Thakore, J.H., Garavan, H., De Sanctis, P. & Foxe, J.J. (2008) Are auditory-evoked frequency and duration mismatch negativity deficits endophenotypic for schizophrenia? High-density electrical mapping in clinically unaffected first-degree relatives and first-episode and chronic schizophrenia. *Biol. Psychiat.*, **64**, 385–391.
Maris, E. & Oostenveld, R. (2007) Nonparametric statistical testing of EEG- and MEG-data. *J. Neurosci. Meth.*, **164**, 177–190.
McLaughlin, D.F. & Kelly, E.F. (1993) Evoked-potentials as indexes of adaptation in the somatosensory system in humans - a review and prospectus. *Brain Res. Rev.*, **18**, 151–206.
Megela, A.L. & Teyler, T.J. (1979) Habituation and the human evoked potential. *J. Comp. Physiol. Psych.*, **93**, 1154–1170.
Mukundan, C.R. (1986) Middle latency components of evoked potential responses in schizophrenics. *Biol. Psychiat.*, **21**, 1097–1100.
Müller, J.R., Metha, A.B., Krauskopf, J. & Lennie, P. (1999) Rapid adaptation in visual cortex to the structure of images. *Science*, **285**, 1405–1408.
Muller-Gass, A., Marcoux, A., Jamshidi, P. & Campbell, K. (2008) The effects of very slow rates of stimulus presentation on event-related potential estimates of hearing threshold. *Int. J. Audiol.*, **47**, 34–43.
Musselwhite, M.J. & Jeffreys, D.A. (1983) Visual evoked potentials to double-pulse pattern presentation. *Vision Res.*, **23**, 135–143.
Nolan, H., Butler, J.S., Whelan, R., Foxe, J.J., Bülthoff, H.H. & Reilly, R.B. (2012) Neural correlates of oddball detection in self-motion heading: a high-density event-related potential study of vestibular integration. *Exp. Brain Res.*, **219**, 1–11.
Olincy, A., Braff, D.L., Adler, L.E., Cadenhead, K.S., Calkins, M.E., Dobie, D.J., Green, M.F., Greenwood, T.A., Gur, R.E., Gur, R.C., Light, G.A., Mintz, J., Nuechterlein, K.H., Radant, A.D., Schork, N.J., Seidman, L.J., Siever, L.J., Silverman, J.M., Stone, W.S., Swerdlow, N.R., Tsuang, D.W., Tsuang, M.T., Turetsky, B.I., Wagner, B.D. & Freedman, R. (2010) Inhibition of the P50 cerebral evoked response to repeated auditory stimuli: results from the Consortium on Genetics of Schizophrenia. *Schizophr. Res.*, **119**, 175–182.
Oostenveld, R., Fries, P., Maris, E. & Schoffelen, J.M. (2011) FieldTrip: Open source software for advanced analysis of MEG, EEG, and invasive electrophysiological data. *Comput. Intell Neurosci.*, **2011**, 156869.
Oranje, B., Wienberg, M. & Glenthoj, B.Y. (2011) A single high dose of escitalopram disrupts sensory gating and habituation, but not sensorimotor gating in healthy volunteers. *Psychiat. Res.*, **186**, 431–436.
Orekhova, E.V., Stroganova, T.A., Prokofyev, A.O., Nygren, G., Gillberg, C. & Elam, M. (2008) Sensory gating in young children with autism: relation to age, IQ, and EEG gamma oscillations. *Neurosci. Lett.*, **434**, 218–223.
Palermo, A., Giglia, G., Vigneri, S., Cosentino, G., Fierro, B. & Brighina, F. (2011) Does habituation depend on cortical inhibition? Results of a rTMS study in healthy subjects. *Exp. Brain Res.*, **212**, 101–107.
Patterson, J.V., Hetrick, W.P., Boutros, N.N., Jin, Y., Sandman, C., Stern, H., Potkin, S. & Bunney, W.E. Jr. (2008) P50 sensory gating ratios in schizophrenics and controls: a review and data analysis. *Psychiat. Res.*, **158**, 226–247.
Pereira, D.R., Cardoso, S., Ferreira-Santos, F., Fernandes, C., Cunha-Reis, C., Paiva, T.O., Almeida, P.R., Silveira, C., Barbosa, F. & Marques-Teixeira, J. (2014) Effects of inter-stimulus interval (ISI) duration on the N1 and P2 components of the auditory event-related potential. *Int. J. Psychophysiol.*, **94**, 311–318.
Perrin, F., Pernier, J., Bertrand, O., Giard, M.H. & Echallier, J.F. (1987) Mapping of scalp potentials by surface spline interpolation. *Electroen. Clin. Neuro.*, **66**, 75–81.
Potter, D., Summerfelt, A., Gold, J. & Buchanan, R.W. (2006) Review of clinical correlates of P50 sensory gating abnormalities in patients with schizophrenia. *Schizophrenia Bull.*, **32**, 692–700.
Rosburg, T., Trautner, P., Elger, C.E. & Kurthen, M. (2009) Attention effects on sensory gating–intracranial and scalp recordings. *NeuroImage*, **48**, 554–563.
Rosburg, T., Zimmerer, K. & Huonker, R. (2010) Short-term habituation of auditory evoked potential and neuromagnetic field components in dependence of the interstimulus interval. *Exp. Brain Res.*, **205**, 559–570.
Roth, W.T., Krainz, P.L., Ford, J.M., Tinklenberg, J.R., Rothbart, R.M. & Kopell, B.S. (1976) Parameters of temporal recovery of the human auditory evoked potential. *Electroen. Clin. Neuro.*, **40**, 623–632.
Sable, J.J., Low, K.A., Maclin, E.L., Fabiani, M. & Gratton, G. (2004) Latent inhibition mediates N1 attenuation to repeating sounds. *Psychophysiology*, **41**, 636–642.
Skrandies, W. & Raile, A. (1989) Cortical and retinal refractory periods in the human visual system. *Int. J. Neurosci.*, **44**, 185–195.
Spencer, K.M., Nestor, P.G., Perlmutter, R., Niznikiewicz, M.A., Klump, M.C., Frumin, M., Shenton, M.E. & McCarley, R.W. (2004) Neural synchrony indexes disordered perception and cognition in schizophrenia. *Proc. Natl. Acad. Sci. USA*, **101**, 17288–17293.
Thoma, R.J., Hanlon, F.M., Huang, M., Miller, G.A., Moses, S.N., Weisend, M.P., Jones, A., Paulson, K.M., Irwin, J. & Cañive, J.M. (2007) Impaired secondary somatosensory gating in patients with schizophrenia. *Psychiat. Res.*, **151**, 189–199.
Wang, A.L., Mouraux, A., Liang, M. & Iannetti, G.D. (2008) The enhancement of the N1 wave elicited by sensory stimuli presented at very short inter-stimulus intervals is a general feature across sensory systems. *PLoS One*, **3**, e3929.
Wang, A.L., Mouraux, A., Liang, M. & Iannetti, G.D. (2010) Stimulus novelty, and not neural refractoriness, explains the repetition suppression of laser-evoked potentials. *J. Neurophysiol.*, **104**, 2116–2124.
Wang, Y., Iliescu, B.F., Ma, J., Josić, K. & Dragoi, V. (2011) Adaptive changes in neuronal synchronization in macaque V4. *J. Neurosci.*, **31**, 13204–13213.
Wastell, D.G. & Kleinman, D. (1980a) Fast habituation of the late components of the visual evoked potential in man. *Physiol. Behav.*, **25**, 93–97.
Wastell, D.G. & Kleinman, D. (1980b) A psychoanatomical investigation of the locus of the mechanism responsible for the refractoriness of the visual vertex potential. *Percept. Psychophys.*, **27**, 149–152.
Wissig, S.C. & Kohn, A. (2012) The influence of surround suppression on adaptation effects in primary visual cortex. *J. Neurophysiol.*, **107**, 3370–3384.
Woldorff, M.G. (1993) Distortion of erp averages due to overlap from temporally adjacent erps - analysis and correction. *Psychophysiology*, **30**, 98–119.
Yeap, S., Kelly, S.P., Sehatpour, P., Magno, E., Javitt, D.C., Garavan, H., Thakore, J.H. & Foxe, J.J. (2006) Early visual sensory deficits as endophenotypes for schizophrenia: high-density electrical mapping in clinically unaffected first-degree relatives. *Arch. Gen. Psychiat.*, **63**, 1180–1188.
Yeap, S., Kelly, S.P., Sehatpour, P., Magno, E., Garavan, H., Thakore, J.H. & Foxe, J.J. (2008a) Visual sensory processing deficits in Schizophrenia and their relationship to disease state. *Eur. Arch. Psy. Clin. N.*, **258**, 305–316.
Yeap, S., Kelly, S.P., Thakore, J.H. & Foxe, J.J. (2008b) Visual sensory processing deficits in first-episode patients with Schizophrenia. *Schizophr. Res.*, **102**, 340–343.
Zucker, R.S. (1989) Short-term synaptic plasticity. *Annu. Rev. Neurosci.*, **12**, 13–31.